Study of the Deoxidation of Steel with Aluminum Wire Injection in a Gas-Stirred Ladle

K. BESKOW, N.N. VISWANATHAN, L. JONSSON, and Du SICHEN

In the present work, the deoxidation of liquid steel with aluminum wire injection in a gas-stirred ladle was studied by mathematical modeling using a computational fluid dynamics (CFD) approach. This was complemented by an industrial trial study conducted at Uddeholm Tooling AB (Hagfors, Sweden). The results of the industrial trials were found to be in accordance with the results of the model calculation. In order to study the aspect of nucleation of alumina, emphasis was given to the initial period of deoxidation, when aluminum wire was injected into the bath. The concentration distributions of aluminum and oxygen were calculated both by considering and not considering the chemical reaction. Both calculations revealed that the driving force for the nucleation of Al_2O_3 was very high in the region near the upper surface of the bath and close to the wire injection. The estimated nucleation rate in the vicinity of the aluminum wire injection point was much higher than the recommended value for spontaneously homogeneous nucleation, 10^3 nuclei/(cm^3/s). The results of the model calculation also showed that the alumina nuclei generated at the vicinity of the wire injection point are transported to other regions by the flow.

I. INTRODUCTION

DEOXIDATION of steel using aluminum wire injection and further removal of inclusions plays a crucial role in ladle metallurgy, especially with the growing demand for cleaner and cleaner steels. There is ongoing interest in understanding the dynamics of inclusions in liquid steel. Deoxidation of steel using aluminum involves three basic consecutive steps: (1) formation of critical nuclei of the deoxidation product, namely, alumina, (2) a progress of deoxidation resulting in the growth of the reaction products, and (3) their separation from the melt. The formation rate of critical nuclei depends on the extent of supersaturation. Further, the growth rate of oxide inclusions is controlled by mass transfer. As the alumina particles are formed, they interact with the bulk flow and local eddy flow of the steel melt and are subject to collision, agglomeration, growth, and flotation. Various models have been developed based on various coarsening and separation mechanisms such as the Stokes collision, turbulent collision, floating separation, *etc.*[1,2] Recently, Tozawa *et al.*[3] have derived an equation for the floating velocity of cluster-shaped alumina inclusions which uses fractal theory for quantification of the size and density of alumina clusters. In order to gain a better understanding of deoxidation phenomena, there is the need to develop a comprehensive model that could involve fluid flow, deoxidation kinetics, and removal of deoxidation products.

Along these lines, a research program has been initiated at the Division of Metallurgy, Royal Institute of Technology (Stockholm). As the first step toward a comprehensive model, the present work involves simulation of the concentration profiles of oxygen and aluminum during deoxidation by aluminum wire injection in a two-dimensional (2-D) gas-stirred ladle.

K. BESKOW, Graduate Student, L. JONSSON, Professor, and DU SICHEN, Associate Professor, are with the Department of Materials Science and Engineering, Division of Metallurgy, Royal Institute of Technology, SE-100 44 Stockholm, Sweden. N.N. VISWANATHAN, Associate Professor, is with the Department of Metallurgical Engineering and Materials Science, Indian Institute of Technology—Bombay, Mumbai - 400 076, India.

Manuscript submitted May 2, 2000.

II. MODEL FORMULATION

The gas-stirred ladle represents a two-phase turbulent recirculating pattern. The mathematical model used in the present study is based on a two-phase model.[4] The gas and liquid phase are considered to be two different interpenetrating and interacting fields. The phases interact with each other at the finite interface areas. The exchanges between phases were represented through source terms in the conservation equations.

The following principal assumptions have been made.

(1) The gas-stirred ladle is axially symmetric; hence, the governing equations can be written in 2-D cylindrical coordinates.
(2) The system is isothermal.
(3) The gas bubble size is constant throughout the domain.
(4) The free surface is assumed to be flat, but allowance is made for the escape of gas at the surface.
(5) The gas is introduced through one calculation cell placed at the center of the ladle-bottom grid plane.
(6) An interface-friction coefficient is used to describe the force between the gas and the liquid phase.
(7) Concentration gradients do not exist at the start of a calculation.
(8) The aluminum wire injection was assumed to have no effect on the flow pattern.
(9) The calculations for the concentration profiles were computed in a transient mode, with time-steps of 0.1 second.
(10) No oxygen transfer occurs across the free surface.

A. *Transport Equations*

The governing equations can be written for mass and momentum, respectively, in the following manner.

Mass conservation of liquid phase

$$\frac{1}{r}\frac{\partial(\alpha_l\rho_l r v_l)}{\partial r} + \frac{\partial(\alpha_l\rho_l w_l)}{\partial z} = 0 \quad [1]$$

Mass conservation of gas phase

$$\frac{1}{r}\frac{\partial(\alpha_g\rho_g r v_g)}{\partial r} + \frac{\partial(\alpha_g\rho_g w_g)}{\partial z} = 0 \quad [2]$$

Total conservation

$$\alpha_l + \alpha_g = 1 \quad [3]$$

Conservation of radial momentum

The conservation equations of radial momentum for the liquid phase and gas phase can be expressed as

$$\frac{1}{r}\frac{\partial(\alpha_p\rho_p r v_p^2)}{\partial r} + \frac{\partial(\alpha_p\rho_p v_p w_p)}{\partial z} = -\alpha_p\frac{\partial P}{\partial r} - \left(\frac{1}{r}\frac{\partial}{\partial r}(\alpha_p r\tau_{rr,p}) + \frac{\partial}{\partial z}(\alpha_p\tau_{rz,p})\right) - F_r \quad [4]$$

where the subscript p stands for l or g, which denote liquid or gas, respectively.

Conservation of axial momentum

Similarly, the conservation equations of axial momentum for the liquid phase and gas phase can be expressed as

$$\frac{1}{r}\frac{\partial(\alpha_p\rho_p r v_p w_p)}{\partial r} + \frac{\partial(\alpha_p\rho_p w_p^2)}{\partial z} = -\alpha_p\frac{\partial P}{\partial z} - \left(\frac{1}{r}\frac{\partial}{\partial r}(\alpha_p r\tau_{rz,p}) + \frac{\partial}{\partial z}(\alpha_p\tau_{zz,p})\right) + \alpha_p\rho_p g - F_a \quad [5]$$

In Eqs. [4] and [5],

$$\tau_{rr,p} = -\mu_{\text{eff}}\left(2\frac{\partial v_p}{\partial r} - \frac{2}{3}(\nabla\cdot\mathbf{v}_p)\right) \quad [6]$$

$$\tau_{rz,p} = -\mu_{\text{eff}}\left(\frac{\partial w_p}{\partial r} + \frac{\partial v_p}{\partial z}\right) \quad [7]$$

$$\tau_{zz,p} = -\mu_{\text{eff}}\left(2\frac{\partial w_p}{\partial z} - \frac{2}{3}(\nabla\cdot\mathbf{v}_p)\right) \quad [8]$$

Again, the subscript p in Eqs. [6] through [8] stands for either the liquid or gas phase.

The radial momentum equations consist of, from the left- to right-hand side, two convective terms, a pressure gradient, a diffusive term, and a friction force term. The axial momentum equations consist of the same terms, but an additional buoyancy term has also been included.

From the conservation equations, it can be seen that the only direct coupling between the gas and liquid velocities is by means of the friction forces F_a and F_r.

B. *Friction Forces*

The friction forces cause transfer of momentum from the slower-moving liquid phase to the faster-moving gas phase. The friction force per unit volume that the liquid exerts upon the gas at the interface is given by Eqs. [9] and [10].

Axial direction

$$F_a = \frac{1}{2}C_D A_D\rho_l(\max(w_{\text{rel}}, w_{\text{con}}))^2 \quad [9]$$

Radial direction

$$F_r = \frac{1}{2}C_D A_D\rho_l(\max(v_{\text{rel}}, v_{\text{con}}))^2 \quad [10]$$

where w_{con} and v_{con} are constant reference values of the velocity difference between the gas and liquid phase in the axial and radial directions, respectively.[5] The drag coefficient (C_D) for a sphere can be expressed by the following expression, suggested by Clift *et al.*:[6]

$$C_D = \frac{24}{\text{Re}}(1 + 0.15\,\text{Re}^{0.678}) + \frac{0.42}{\left(1 + \frac{4.25\cdot 10^{-4}}{\text{Re}^{1.16}}\right)} \quad [11]$$

The equivalent spherical bubble diameter of the gas bubbles was calculated using an empirical equation determined by Mori *et al.*:[7]

$$d_B = \left(\left(\frac{6\gamma_l D_{i,n}}{\rho_l g}\right)^2 + 0.0242\,(q_g^2 D_{i,n})^{0.867}\right)^{1/6} \quad [12]$$

C. *Turbulent Transport Equations*

The equations used for calculating the turbulent kinetic energy (k) and the dissipation rate (ε) are from the k-ε model,[8] which enables the computation of the effective viscosity (μ_{eff}) in Eqs. [6] through [8]. The consideration that the presence of a dispersed phase (in this case, gas) in a bulk phase (in this case, liquid) lowers the values of the turbulent kinetic energy and the energy dissipation, as shown by Hamill and Malin,[9] has been incorporated in this model using the source terms S_k and S_ε. Details of the k-ε model and the model parameters can be found in earlier publications.[8,9]

D. *Boundary Conditions*

Argon gas is injected through the gas inlet, which is placed in the center at the bottom of the ladle.

1. *Gas inlet*

Only an axial gas velocity exists in the calculation cell of the gas inlet. The turbulent kinetic energy (k_{in}) and the energy dissipation rate (ε_{in}) were calculated according to the following formulas:[5]

$$k_{in} = 0.1193 w_{g,in}^2 \quad [13]$$

$$\varepsilon_{in} = 1.476\frac{w_{g,in}^3}{D_{i,n}} \quad [14]$$

2. *Ladle bottom/ladle wall*

At the ladle bottom, all velocities are set to zero; *i.e.*, a no-slip boundary condition is imposed for the momentum equation. In the grids closest to the ladle bottom, logarithmic wall functions are used to calculate the shear stresses, turbulent kinetic energy, energy dissipation, and the velocity components parallel to the ladle bottom.[10]

3. *Surface*

The free surface is assumed to be flat, frictionless, and impervious to liquid; however, gas is allowed to leave the system at the rate at which it arrives.

4. *Furnace axis*

The following boundary conditions are used at the furnace axis: zero radial velocities at the axis and a zero gradient of axial velocity in the radial direction.

E. *Computation of Concentration Profiles*

The deoxidation reaction can be expressed as follows:

$$2[\mathrm{Al}]_{\mathrm{Metal}} + 3[\mathrm{O}]_{\mathrm{Metal}} = \mathrm{Al_2O_3\ (solid)}$$
$$\Delta G^\circ = -1{,}209{,}490 + 391.4T \quad \mathrm{J} \qquad [15]$$

It is expected that if the supersaturation of the melt with the reactants is not substantial, Reaction [15] can only be initiated after a certain incubation period, which is required for the homogeneous nucleation of alumina. In order to examine the driving force for the homogeneous nucleation and further the nucleation rate of the reaction product, computations were carried out without considering the chemical reaction to form alumina at the initial stages of the deoxidation. On the other hand, it is also expected that the deoxidation reaction is very fast at the steelmaking temperature, so that the process is essentially controlled by mass transfer in the liquid metal after the nucleation period. Hence, calculations by assuming local thermodynamic equilibrium in each cell at each given instance were also performed.

After obtaining a steady flow pattern, the concentration profiles of O, Al, and Al_2O_3 were computed in transient mode. These equations have the following general form:

$$\frac{\partial(\alpha_l \rho_l C_i)}{\partial t} + \mathrm{div}\,(\alpha_l \rho_l \mathbf{u}_l C_i - \alpha_l \Gamma_{C_i}\,\mathrm{grad}\,C_i) = \alpha_l S_{C_i} \qquad [16]$$

Equation [16] consists of, from left to right, a time-dependence term, a convection term, a diffusion term, and a source term. In the case of the calculation without consideration of the chemical reaction, only the conservation equations for O and Al were used. When the deoxidation reaction was incorporated, the conservation equation for Al_2O_3 was introduced. The three conservation equations were identical except for the property-related coefficients. It should be pointed out that the produced Al_2O_3 due to deoxidation is in solid form. However, the solid Al_2O_3 particles were not considered as a separate phase in this work, since they would not affect the mass transfer in the liquid phase to an appreciable extent.

The diffusion coefficients used for Al and O in liquid iron are[11]

$$D_{\mathrm{Al}} = 0.35 \cdot 10^{-8} \quad (\mathrm{m^2/s}) \qquad [17]$$

$$D_{\mathrm{O}} = 33.4 \cdot 10^{-8} \exp\left(-\frac{50{,}200}{RT}\right) \quad (\mathrm{m^2/s}) \qquad [18]$$

F. *Source Terms for Deoxidation Reaction*

While the source/sink term for Al consists of both the part due to the aluminum addition and the part due to the chemical Reaction [15], the source/sink terms for O and Al_2O_3 only have the contribution of Reaction [15]. In the case of the calculations without considering Reaction [15], the contribution to the source/sink terms from the chemical reaction would be zero.

Table I. Interaction Coefficients[12]

e_i^j	Element j		
Element i	Al	C	O
Al	0.048	0.11	−1.60
O	−0.94	−0.13	−0.20

1. *Aluminum wire injection*

A simple model has been used for aluminum wire injection. The aluminum wire is expected to travel some distance in the molten steel before it becomes completely molten. Using a one-dimensional unsteady conduction equation along the radial direction of the wire, it is possible to estimate the time for the wire to reach its melting point. For a 15 mm wire, this time was estimated to be 0.11 seconds. The product of the time to reach the melting point and the velocity of the wire injection gives the estimation for the aluminum wire depth in the molten steel. In the present work, the aluminum addition has been modeled by a constant source term (kg m^{-3} s^{-1}) of aluminum from the estimated wire volume in the steel bath.

2. *Deoxidation*

When chemical Reaction [15] is considered, the source/sink terms for O, Al, and Al_2O_3 have been calculated assuming local thermodynamic equilibrium. In the case of oxygen, the source term is expressed as

$$\mathrm{Source[O]} = \rho_l / \Delta t \cdot (C_{\mathrm{O}}^{i,1} - C_{\mathrm{O}}^{i,0}) \qquad [19]$$

where the superscripts i,0 and i,1 denote the instants at the beginning and end of time-step i. The source terms for Al and Al_2O_3 can be determined from Eq. [19] using appropriate stoichiometric factors. In the case of Al, the rate of the addition of aluminum should also be added in the source term.

The equilibrium constant (k_{eq}) for Reaction [15] can be described as

$$k_{eq} = \frac{a_{\mathrm{Al_2O_3}}}{(\mathrm{(wt\ pct\ Al)}f_{\mathrm{Al}})^2\,(\mathrm{(wt\ pct\ O)}f_{\mathrm{O}})^3} \qquad [20]$$

where f_{Al} and f_{O} are the activity coefficients of Al and O, respectively, and can be expressed by

$$\mathrm{Log}_{10}\, f_{\mathrm{Al}} = e_{\mathrm{Al}}^{\mathrm{Al}} \cdot \mathrm{(wt\ pct\ Al)} + e_{\mathrm{Al}}^{\mathrm{C}} \cdot \mathrm{(wt\ pct\ C)} + e_{\mathrm{Al}}^{\mathrm{O}} \cdot \mathrm{(wt\ pct\ O)} \qquad [21]$$

$$\mathrm{Log}_{10}\, f_{\mathrm{O}} = e_{\mathrm{O}}^{\mathrm{Al}} \cdot \mathrm{(wt\ pct\ Al)} + e_{\mathrm{O}}^{\mathrm{C}} \cdot \mathrm{(wt\ pct\ C)} + e_{\mathrm{O}}^{\mathrm{O}} \cdot \mathrm{(wt\ pct\ O)} \qquad [22]$$

The adopted interaction coefficients[12] are listed in Table I.

Conservation equations, including the k-ε model along with Eqs. [20] through [22], were solved simultaneously to obtain the velocity vectors, the turbulent kinetic energy, the dissipation rate, the effective viscosity, and the concentrations of Al, O, and Al_2O_3. The governing equations were solved using the Phoenics commercial computational fluid

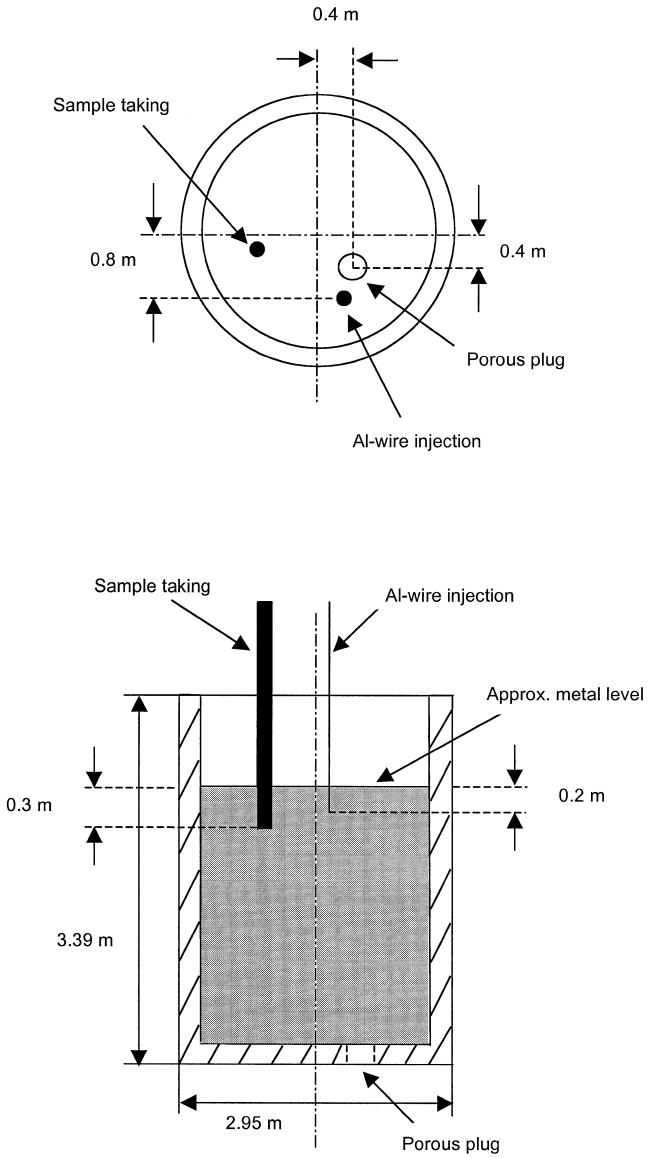

Fig. 1—Schematic drawing of the experimental ladle.

dynamics (CFD) code. Appropriate grid refinement was applied near the gas inlet, walls, and free surface.

III. INDUSTRIAL TRIALS

Experiments were conducted at Uddeholm Tooling AB (Hagfors, Sweden) to determine the aluminum and oxygen contents in the molten steel in an argon gas–stirred ladle during deoxidation with aluminum wire injection. The ladle furnace (from ASEA, rebuilt 1991 by Centromet) consists of a 70-ton ladle equipped with an inductive stirrer and with two porous plugs for argon gas stirring. In the present investigation, only one porous plug was used. The geometry of the furnace, along with the positions of aluminum-adding and sample-taking, is schematically shown in Figure 1. While Uddeholm usually uses inductive stirring in their deoxidation process, only gas stirring with argon gas was utilized in the present trial study. After tapping of the electric arc furnace (EAF), the ladle was taken to the ladle furnace. A steel sample was taken immediately after the arrival of the ladle. This was followed by removal of the slag. When the slag had been removed, the steel was deoxidized by injection of aluminum wire. The wire was injected from the top of the ladle (Figure 1). The amount of aluminum injected was 30 kg. The time required for the injection was about 30 seconds. A steel sample was taken just before the aluminum wire injection. More samples were taken after the injection. Measurements of the oxygen potential and the temperature of the steel were carried out at the same time. The oxygen potential in the molten steel was measured using an oxygen sensor with Cr/Cr_2O_3 as the reference electrode. The position of the oxygen and temperature sensors is the same as the sample-taking position. In the evaluation of oxygen potentials, correction for electronic conduction was made using the software supplied by the sensor company. The steel samples were analyzed with emphasis on the total O and Al contents of the steel. The oxygen was analyzed by combustion analysis, and Al was analyzed using optical emission spectrometry.

Table II. Input Data for the Mathematical Model Simulation

Parameter	Value
Ladle diameter (m)	2.8
Liquid bath height (m)	2.34
Gas inlet diameter (m)	0.009
Diameter of aluminum wire (m)	0.015
Gas flow rate (N L/min)	80
Aluminum wire velocity (m/s)	2.2
Temperature (K)	1773
Initial concentrations:	
wt pct C	0.80
ppm O	40

The input data for the present model, listed in Table II, are based on those used in the industry. However, it should be pointed out that while the gas flow rate used for the model calculation was the same as in the industrial operation, the porous plug for argon injection in the real ladle was not along the central line. On the other hand, as the first step of the research program, the argon injection was assumed to be along the central axis of the ladle in the present calculation, so that the flow field could be treated as 2-D.

IV. RESULTS AND DISCUSSION

A. *Flow in the Ladle*

The calculated flow patterns clearly depict the well-reported recirculation pattern in a gas-stirred ladle. (For the sake of brevity, the flow patterns are not presented in this article, but can be supplied on request.) The friction force between the gas and metal together with the buoyant force from the bubbles results in high velocities at the center of the ladle. At the vicinity of the nozzle, ascending bubbles drag liquid steel toward the center and lift it upward. The velocity of the molten steel at the surface of a ladle with a gas input of 80 NL/min is about 0.4 to 0.5 m/s, which is in line with the measured surface velocities.[13]

After obtaining the steady flow pattern, concentration profiles of O, Al, and Al_2O_3 were computed in transient mode by assuming either local thermodynamic equilibrium in each

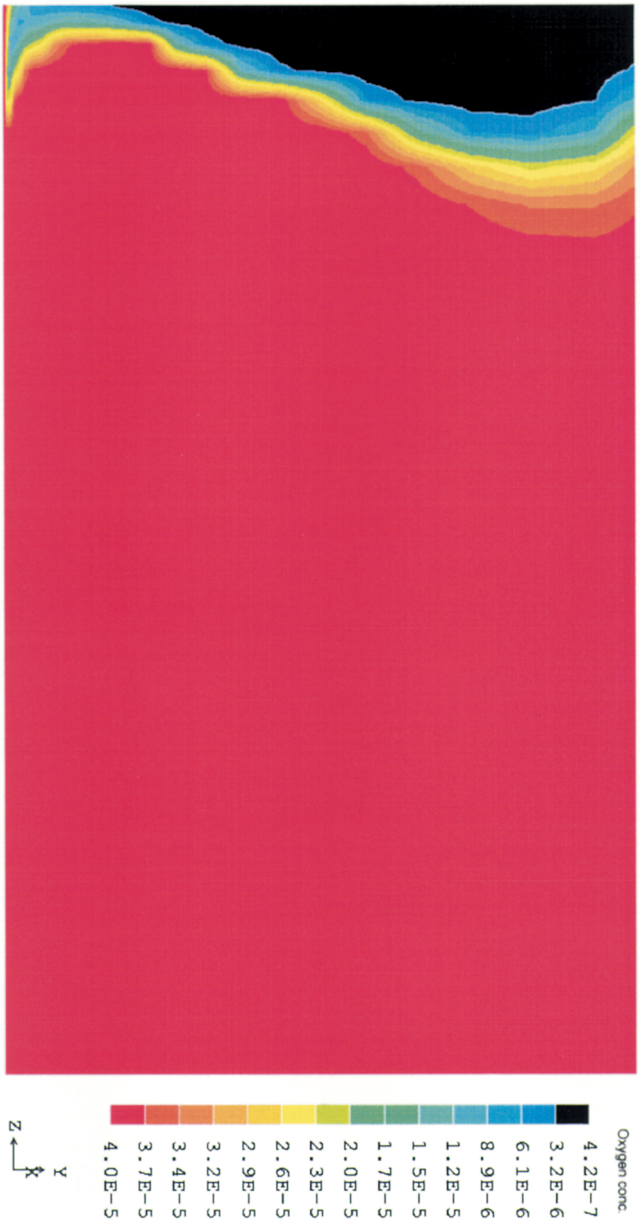

Fig. 2—Oxygen concentration during aluminum wire injection, time = 5 s.

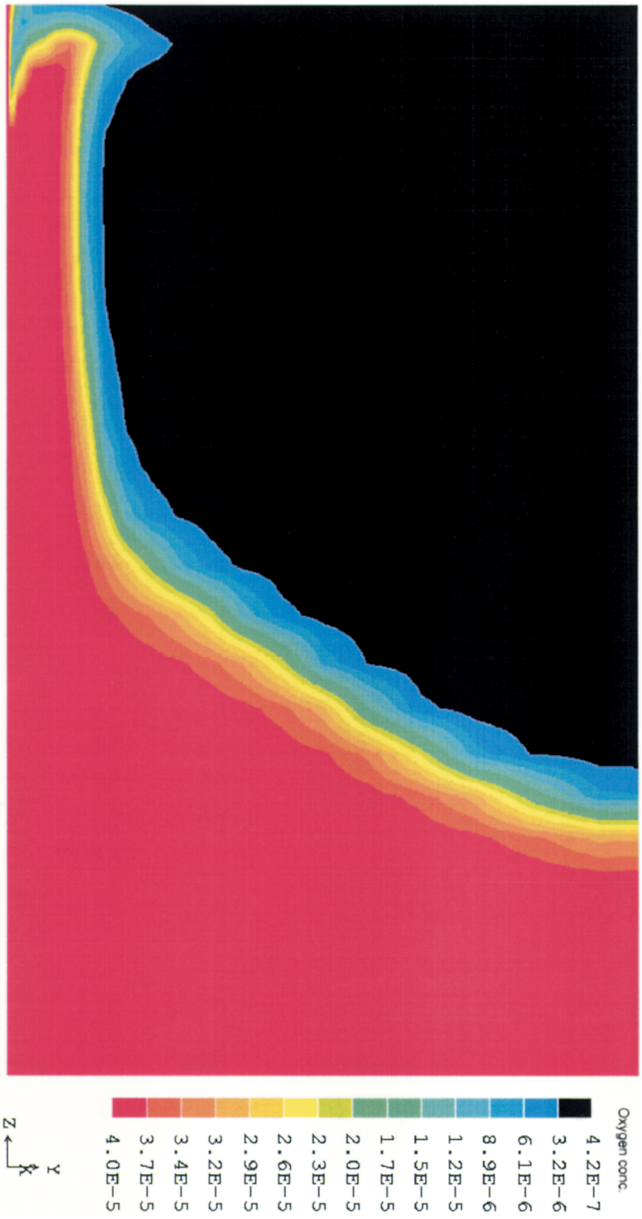

Fig. 3—Oxygen concentration at the end of wire injection, time = 30 s.

cell at each given instance or no chemical reaction. The latter calculation was only performed to study the driving force for the nucleation of alumina in the initial stages.

B. *Calculation Based on Local Thermodynamic Equilibrium*

The initial mass concentration of dissolved oxygen in the molten steel was 40 ppm. During the transient computation, it was assumed that the flow pattern was not affected by the introduction of aluminum wire. The present computations were made for the introduction of aluminum at the center of the ladle, in order to keep the 2-D symmetry. Aluminum wire injection away from the centerlines demands computation of concentration profiles in three dimensions, which will be done in our future work. Figures 2 and 3 show the computed concentration profiles of oxygen during the introduction of aluminum wire after 5 and 30 seconds, respectively. The concentration profiles clearly show that the oxygen concentration propagates through the molten steel in accordance with the recirculation pattern. The aluminum wire injection was terminated after 30 seconds. It should be pointed out that concentration gradients even exist in the upper region close to the wall and in the lower-center region. Since the concentration gradients in these two regions are small, they cannot be shown by the color scale in these figures.

Figures 4 and 5 show the concentration profiles of aluminum during the introduction of aluminum wire after 5 and 30 seconds, respectively. It was found that, very close to the wire injection zone, the concentration of aluminum is very high. This suggests that if the introduction of aluminum wire is faster compared to the rate at which aluminum is transported away from the wire-feeding zone, molten aluminum formed may rise toward the molten steel surface. The

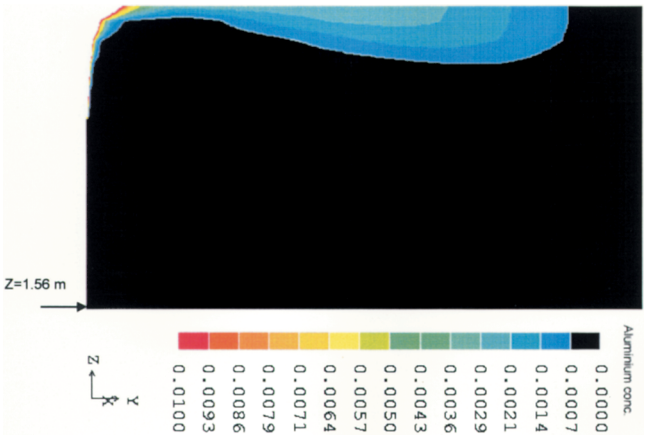

Fig. 4—Aluminum concentration during wire injection, time = 5 s. The figure represents the upper 1/3 of the ladle.

Fig. 5—Aluminum concentration at the end of wire injection, time = 30 s.

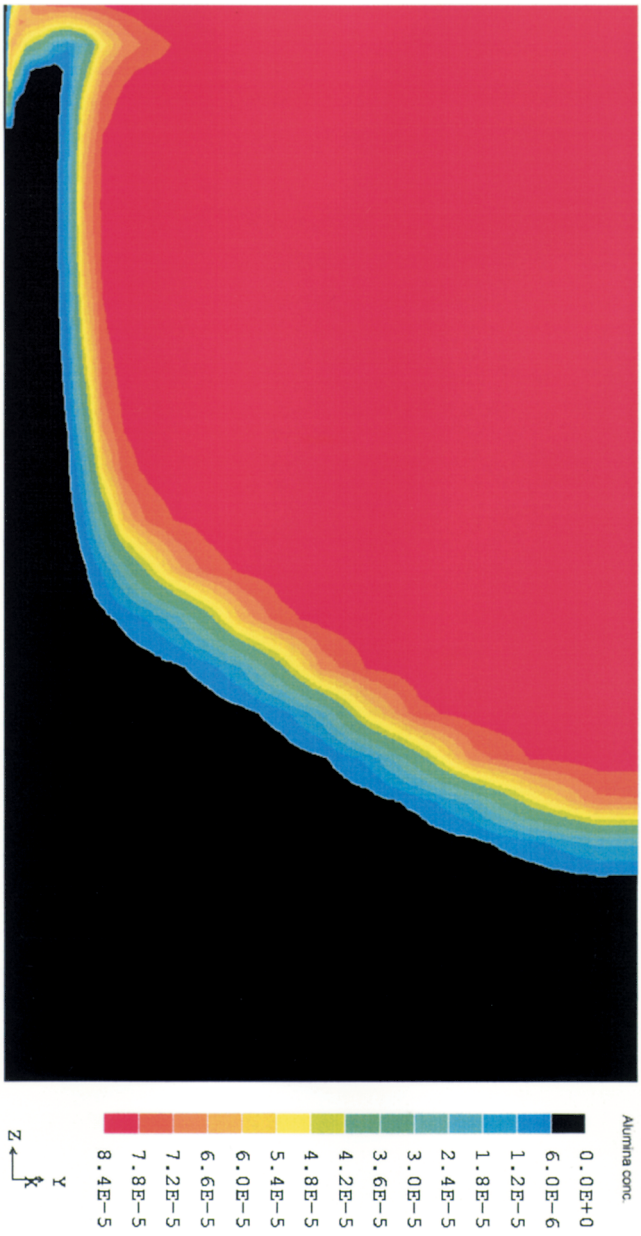

Fig. 6—Alumina concentration at the end of wire injection, time = 30 s.

concentration profile shows clearly that the steel supersaturated with aluminum propagates according to the recirculation pattern. These results are in accordance with the calculated concentration patterns of alumina, shown in Figure 6.

Figure 7 and 8 show the O and Al concentrations after the wire injection has been terminated. During this period, the excess aluminum becomes gradually distributed and reacts with the remaining oxygen.

Figure 9 shows the change, with time, in average O concentration in the steel for two different flow rates: 80 and 120 N L/min, respectively. The figure shows that during the initial stages of wire injection, the overall deoxidation rate is at the same level for both flow rates, while the higher flow rate leads to a slightly higher deoxidation rate. However, as the aluminum concentration front penetrates deeper into the melt, the overall deoxidation rate is influenced by the flow

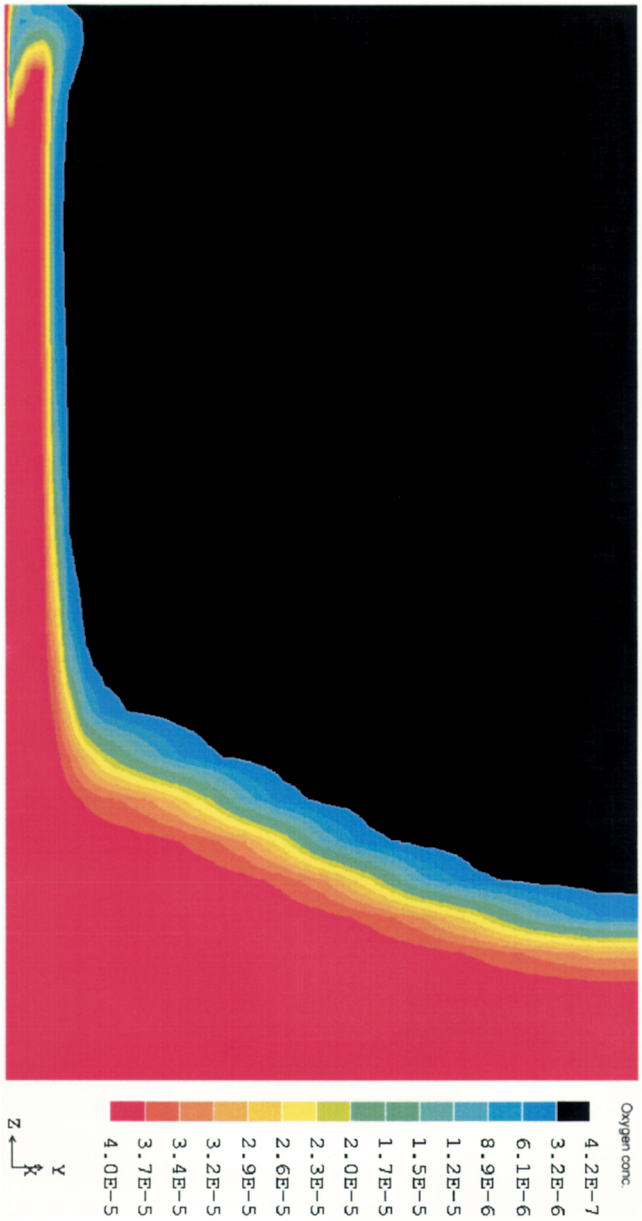

Fig. 7—Oxygen concentration after wire injection, time = 50 s.

Fig. 8—Aluminum concentration after wire injection, time = 50 s.

rate. During the initial stages, both the oxygen and aluminum concentrations are high. The high driving force due to the differences between the prevailing and the equilibrium concentrations of oxygen and aluminum would play a dominating role in the initial stages of the process. At later stages (after about 20 seconds), the deoxidation rate becomes more dependent on the gas flow rate. In these stages, even the mixing due to the turbulent field would have a strong impact on the deoxidation rate. While it takes roughly 10 minutes to obtain a uniform concentration, the variation of the concentration with time is very slow after 30 to 40 seconds.

Based on the total aluminum added during industrial trials and the compositions of steel samples taken, the time for complete mixing was estimated. The mass-balance calculation regarding the aluminum content revealed that the average aluminum concentration after complete mixing would be 0.046 mass pct Al. The chemical analyses in the steel samples taken after 2 and 5 minutes showed that the steel contained 0.064 and 0.044 mass pct Al (total), respectively. The higher aluminum concentration in the sample taken after 2 minutes, as compared to the value based on the mass-balance calculation, indicates that the steel bath has not reached a uniform composition. On the other hand, the Al concentration in the sample taken after 5 minutes is very close to the value of 0.046 mass pct Al, implying that the mixing is nearly complete. These results are in agreement with the results of the model calculation. In the case of oxygen contents, the probe showed an oxygen potential of 10 ppm after 30 seconds in the experiments starting with a steel melt having 38 ppm oxygen. This is in good agreement with the model prediction shown in Figure 9. However, it is noted that the results of these plant experiments compare with the present modeling results only in a semiquantitative sense. This is due to the difficulties involved in the trial investigation. For example, there were uncertainties involved in the gas flow rate due to leakage of gas from the

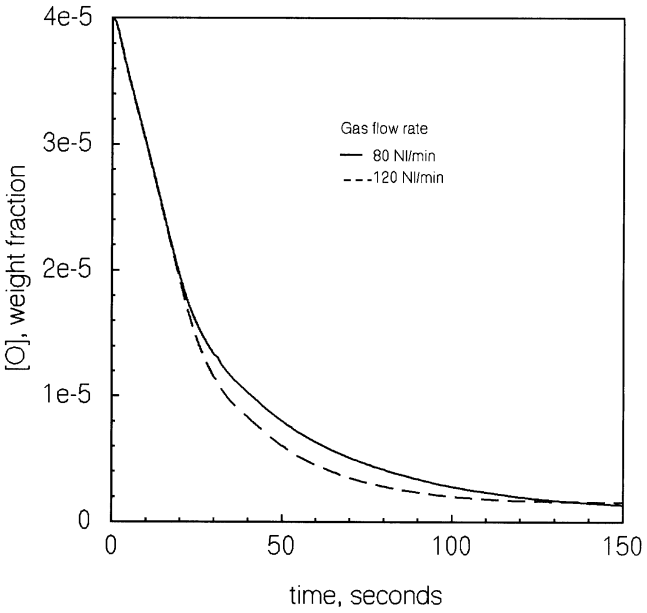

Fig. 9—Average oxygen concentration in weight fraction as a function of time.

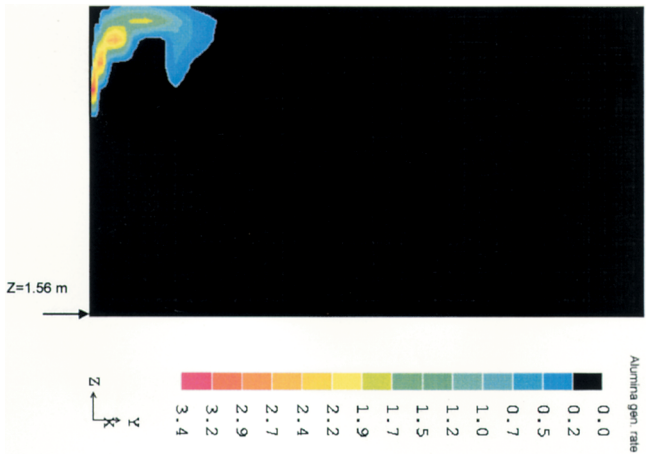

Fig. 10—Contours of rate of generation of alumina (kg m^{-3} s^{-1}), time = 30 s. The figure represents the upper 1/3 of the ladle.

porous plugs. The aluminum wire feeding rate was also not constant. Well-documented plant trials are necessary for further validation of the present modeling. Furthermore, the 2-D model used places the porous plug in the center of the ladle. The difference in the location of the gas inlet between the industrial ladle and the ladle used to build up the mathematical model would also make the comparison semi-quantitative.

The previously discussed results (Figures 2 through 9) were computed by assuming local thermodynamic equilibrium. Representation of the rate of formation of alumina based on nucleation kinetics can give better insight into the distribution of the radius of critical nuclei in the steel bath. However, present computations show that during injection, most of the alumina production occurs close to the vicinity of the aluminum wire injections. This has been illustrated in Figure 10, which shows the rate of alumina production

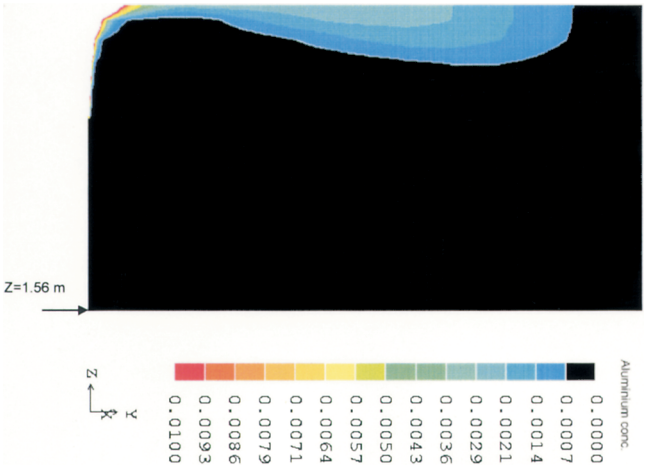

Fig. 11—Aluminum concentration during wire injection, without considering the chemical reaction, time = 5 s. The figure represents the upper 1/3 of the ladle.

at the end of the wire injection. At the vicinity of the aluminum wire injection, the outflow of oxygen-free steel is substituted by the fresh supply of oxygen from the upcoming steel from the center of the bath.

C. *Calculation of the Driving Force for Nucleation*

It is possible to estimate the homogeneous nucleation rate of the reaction product from the extent of supersaturation of the melt with reactants. For this, computations were carried out without considering the chemical reaction to form alumina. Figure 11 shows the calculated aluminum distribution after 5 seconds. It is seen that the concentration distribution is very similar to the aluminum distribution shown in Figure 4. The similarity between the aluminum distributions calculated with and without considering Reaction [15] is because of the low initial oxygen content. The local concentration of oxygen is not sufficient to consume the dissolved aluminum to an appreciable extent. Figure 11 also confirms that the driving force for the nucleation of Al_2O_3 in the vicinity of the aluminum wire injection point is indeed very high. Even in the area close to the upper surface of the bath, the supersaturation of aluminum is sufficiently high to ensure the nucleation of alumina.

Knowing the concentration of aluminum, it is possible to estimate the maximum nucleation rate, given by[14]

$$I = A_0 \exp\left(-\Delta F^*/RT\right) \qquad [23]$$

where A_0 is constant at approximately 10^{27} nuclei/(cm^3/s) and ΔF^* is the free energy of activation, defined by

$$\Delta F^* = \frac{16\pi\gamma^3}{3(\Delta F_v)^2} \qquad [24]$$

where ΔF_v = [25]

$$\frac{\Delta F_m \text{ (molar free energy change of Reaction [15])}}{V_m \text{ (molar volume of the new phase)}}$$

The estimation of the nucleation rate showed that, at the vicinity of the aluminum wire injection, the nucleation rate is much higher than the recommended value for spontaneously homogeneous nucleation (nucleation takes place as soon as

the aluminum wire is injected), which is 10^3 nuclei/(cm^3/s).[14] This suggests that the spontaneous reaction assumed in the present model is reasonable during wire injection. In other words, the present modeling results are expected to be close to the real situation in the vicinity of the wire injection. The alumina nuclei generated in the vicinity of the wire injection are transported to other regions by the flow, and they grow as they travel in the steel melt. The growth of alumina particles is expected to play an important role during later stages of deoxidation. Present modeling results give some insight into the nucleation of alumina during deoxidation, especially in terms of the generation of nucleation close to the wire injection. This information could possibly be used for controlling the number and size of nuclei by varying the wire injection rate as well as making use of multiple wire injections at different locations. After the formation of nuclei, the concentrations of [Al] and [O] have been brought to a lower level. Consequently, the mass transfer becomes even more important at this stage and is expected to be the rate-controlling step. Hence, the calculation assuming thermodynamic equilibrium, which was discussed in the previous section, would provide a more reasonable description for the later stages of the deoxidation.

It should be mentioned that as the alumina particles are generated, they collide, agglomerate, and float to the steel surface or stick on the walls. In the present model, agglomeration and removal of alumina particles have not been considered. Modification of the present model to incorporate inclusion growth and separation will be considered for our future communications. Modifications such as (1) increasing the dimension of the model from 2-D to three-dimensional, (2) modification of the deoxidation reaction model to consider nucleation and growth, and (3) modification of the model to consider flotation of particles are necessary for a better representation of the deoxidation process.

V. SUMMARY

Some aspects of the deoxidation of liquid steel using aluminum wire injection in a gas-stirred ladle have been simulated. The fluid flow was simulated using a two-phase model. In order to study the driving force for the nucleation of alumina, the mass transfer of Al has been calculated both by considering and not considering the deoxidation reaction that forms Al_2O_3. The former calculation has been done assuming local thermodynamic equilibrium. To verify the model prediction, industrial trials have been carried out at Uddeholm Tooling AB. The experimental results have been found to agree with the model calculation within the uncertainties of the industrial trials. The results of the simulation have shown that most of the alumina is generated close to the vicinity of the wire injection region during wire injection. Further modification in the present model incorporating nucleation, growth, and removal are necessary for a deeper insight into the deoxidation phenomena.

ACKNOWLEDGMENTS

The authors thank Professors S. Seetharaman and P. Jönsson for their comments on this work. The authors also thank Uddeholm Tooling AB (Hagfors, Sweden) for providing the facility of the industrial trial study. The assistance in carrying out the experimental study obtained from MSc. Henrik Issal is appreciated. Financial support for this work from the Swedish Council for Technical Science (TFR) is gratefully acknowledged.

NOMENCLATURE

a_i	activity of element i
A_D	projected area per unit volume (L/m)
A_0	constant in equation for maximum nucleation rate
C_D	drag coefficient
C_i	concentration of element i, weight fraction
d_B	diameter of gas bubble (m)
D_{Al}	diffusion coefficient for aluminum (m^2/s)
$D_{i,n}$	inner diameter of gas inlet (m)
D_O	diffusion coefficient for oxygen (m^2/s)
e_i^j	interaction coefficient
f_i	activity coefficient for element i
F_a	friction force in the axial direction that the liquid exerts upon the gas at the interface per unit volume (N/m^3)
F_r	friction force in the radial direction that the liquid exerts upon the gas at the interface per unit volume (N/m^3)
ΔF_v	free energy per volume (J/m^3)
ΔF^*	activation energy (J/mole)
ΔF_m	molar free energy (J/mole)
g	gravitational acceleration (m/s^2)
I	maximum nucleation rate ($1/cm^3$ s)
k_{eq}	equillibrium constant
k_{in}	turbulent kinetic energy at inlet (J/kg)
P	pressure (N/m^2)
q_g	gas flow rate (m^3/s)
r	radial distance (m)
R	gas constant (J/mole K)
Re	Reynold's dimensionless number
S_{C_i}	source rate of C_i (kg/m^3 s)
S_ε	source term in turbulence equation (kg/m s^3)
S_g	source term in turbulence equation (kg/m s^4)
t	time (s)
T	temperature (K)
$\mathbf{u}_l$	velocity vector of liquid phase (m/s)
v_{con}	reference value for v_{rel} (m/s)
v_g	radial velocity component of the gas (m/s)
v_l	radial velocity component of the liquid (m/s)
$\mathbf{v}_p$	velocity vector where p stands for either liquid (l) or gas (g) phase (m/s)
v_{rel}	relative velocity difference between gas and liquid in radial direction (m/s)
V_m	molar volume (m^3/mole)
w_{con}	reference value for w_{rel} (m/s)
w_g	axial velocity component of the gas (m/s)
$w_{g,in}$	axial velocity component for gas phase at gas inlet (m/s)
w_l	axial velocity component of the liquid (m/s)
w_{rel}	relative velocity difference between gas and liquid in axial direction (m/s)
z	axial distance (m)
α_l	volume fraction of liquid
α_g	volume fraction of gas
ε_{in}	dissipation rate of turbulent kinetic energy at gas inlet (m^2/s^3)

γ	surface tension (N/m)
γ_l	surface tension of liquid (N/m)
μ_{eff}	effective viscosity (kg/m s)
ρ_g	density of the gas (kg/m^3)
ρ_l	density of the liquid (kg/m^3)
$\tau_{rr,p}$	component of the stress tensor where p stands for either liquid (l) or gas (g) phase
$\tau_{rz,p}$	component of the stress tensor where p stands for either liquid (l) or gas (g) phase
$\tau_{zz,p}$	component of the stress tensor where p stands for either liquid (l) or gas (g) phase
Γ_{C_i}	exchange coefficient of the entity c in the phase

REFERENCES

1. S. Taniguchi and A. Kikichi: *Tetsu-to-Hagané*, 1992, vol. 78, pp. 527-35 (in Japanese).
2. S. Taniguchi, A. Kikichi, T. Ise, and N. Shoji: *Iron Steel Inst. Jpn.*, 1996, vol. 36, pp. S117-S120.
3. H. Tozawa, Y. Kato, K. Sorimachi, and T. Nakanishi: *Iron Steel Inst. Jpn.*, 1999, vol. 39, pp. 426-34.
4. D.B. Spalding: *Mathematical Modelling of Fluid Mechanics, Heat-Transfer and Chemical Reaction Processes*, A Lecture Course, Imperial College CFDU Report No. HTS/80/1, Imperial College, London, England.
5. P. Jönsson and L. Jonsson: *Scand. J. Metall*, 1995, vol. 24, pp. 194-206.
6. R. Clift, J.R. Grace, and M.E. Weber: *Bubbles, Drops and Particles*, Academic Press Inc., New York, NY, 1989.
7. K. Mori, M. Sano, and T. Sato: *Iron Steel Inst. Jpn. Int.*, 1979, vol. 19, pp. 553-58.
8. B.E. Launder and D.B. Spalding: *Mathematical Models of Turbulence*, Academic Press, London, 1972.
9. I.S. Hamill and M.R. Malin: *PHOENICS J.*, 1991, vol. 4, suppl. 2, p. 212.
10. B.E. Launder and D.B. Spalding: *Comp. Meth. Appl. Mech. Eng.*, 1974, p. 269.
11. Y. Kawai and Y. Shiraishi: *Handbook of Physico-Chemical Properties at High Temperatures*, ISIJ, Tokyo, 1988.
12. J.F. Elliot, M. Gleiser, and V. Ramakrishna: *Thermochemistry for Steelmaking*, Addison-Wesley Publ. Co., Reading, MA, 1963, vol. 2.
13. T.C. Hsiao: MF 79063 E/2, MEFOS, Luleå, Sweden, 1979.
14. Hong Yong Sohn and Milton E. Wadsworth: *Rate Processes of Extractive Metallurgy*, Plenum Press, New York, NY, 1979, p. 399.